

Advancing Technology for Starlight Suppression via an External Occulter

N. J. Kasdin^a, D. N. Spergel^a, R. J. Vanderbei^a, D. Lisman^b, S. Shaklan^b, M. Thomson^b, P. Walkemeyer^b, V. Bach^b, E. Oakes^b, E. Cady^b, S. Martin^b, L. Marchen^b, B. Macintosh^c, R. E. Rudd^c, J. Mikula^d, D. Lynch^d

^aPrinceton University, Princeton, NJ, 08544 USA

^bJet Propulsion Laboratory, California Institute of Technology, Pasadena, CA, 91109 USA

^cLawrence Livermore National Laboratory, Livermore, CA, 94551 USA

^dNASA Ames Research Center, Moffett Field, CA, 94035 USA

ABSTRACT

External occulters provide the starlight suppression needed for detecting and characterizing exoplanets with a much simpler telescope and instrument than is required for the equivalent performing coronagraph. In this paper we describe progress on our Technology Development for Exoplanet Missions project to design, manufacture, and measure a prototype occulter petal. We focus on the key requirement of manufacturing a precision petal while controlling its shape within precise tolerances. The required tolerances are established by modeling the effect that various mechanical and thermal errors have on scatter in the telescope image plane and by suballocating the allowable contrast degradation between these error sources. We discuss the deployable starshade design, representative error budget, thermal analysis, and prototype manufacturing. We also present our metrology system and methodology for verifying that the petal shape meets the contrast requirement. Finally, we summarize the progress to date building the prototype petal.

Keywords: External occulters, occulters, starshades, exoplanets, high-contrast imaging

1. INTRODUCTION

This paper describes our progress toward completing the external occulter milestone in support of the the ROSES Technology Development for Exoplanet Missions (TDEM) program, part of NASA's Exoplanet Exploration Program. Our goal is to advance the readiness of on of the most challenging technologies associated with occulter-based planet finding and characterization—manufacturing a large starshade to the needed accuracy.* *Our objective is to, for the first time, build a full-scale occulter petal, using flight-like processes and materials, and to near-flight tolerances as they are presently understood.* We will perform metrology to confirm that the critical shape requirements are satisfied and a modeled prediction of the resulting starlight suppression reaches our goal.

There are, of course, many other critical engineering technologies that need to be studied and verified to eventually have confidence in the success of an occulter mission. Principal among them are deployment accuracy, occulter position sensing and formation flying, thermal and dynamic stability, optical scatter off the edge (solar glint), validated optical modeling, and design reference mission analyses with algorithms for planet identification. We postpone all of these to future studies, though the design we are using is a flight design whose kinematics have been demonstrated in a preliminary deployment test.

Building and measuring a petal, as we do in this TDEM study, addresses one of the most critical aspects of starshade manufacture—the petals, with their sharp and precisely defined edges, are responsible for diffracting starlight away from the receiving telescope while the telescope looks slightly off to the side of the occulter to see a planet. Quantitatively, our established milestone for this TDEM study is stated as follows:

Send correspondence to jkasdin@princeton.edu

*In this paper we use *occulter* to refer to the entire spacecraft while we use *starshade* to refer to the deployable mechanical payload providing the suppression.

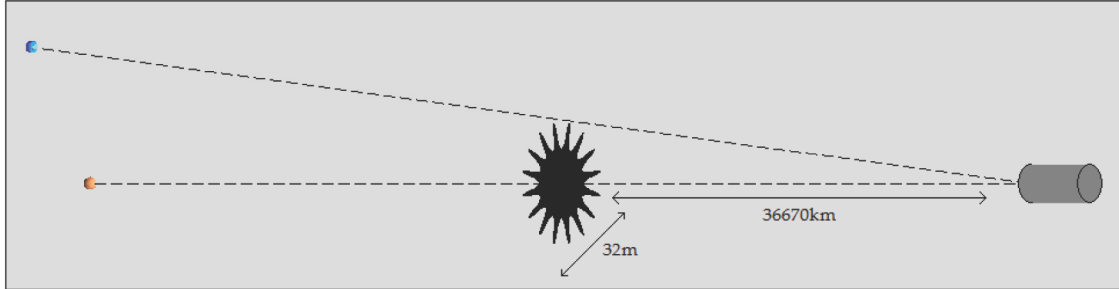


Figure 1. A schematic diagram of a representative occulter flying in formation with a telescope to provide starlight suppression and enable imaging of a companion exoplanet at a small geometric inner working angle.

On a single full-scale petal made of flight-like materials, measure the width of the optical edges at a sufficient number of locations and with sufficient accuracy to show that, using modeling, the mean contrast in the image plane from a uniform field propagated past an occulter with petals of the measured shape in an annulus of width equal to the full-width half-max of the telescope point spread function at the smallest inner working angle is 3×10^{-10} or better, the allocated contrast to static errors. We repeat the measurements and analysis a sufficient number of times to give 95% confidence that the predicted contrast is correct.

We note that this objective conforms to the allocated error for an occulter mission designed for a total contrast, due to all errors, of 1×10^{-9} . A relaxed contrast number such as this is typical of most first TDEMs. Nevertheless, all indications point to our achieving a much more aggressive goal of 2×10^{-11} , consistent with a mission contrast of 10^{-10} . The remainder of this paper describes the design of the occulter we are testing (Section 2), the error analysis supporting the requirements (Section 3), the occulter mechanical design (Section 4), the metrology approach (Section 5), and our progress toward completing the milestone (Section 6).

2. BACKGROUND AND DESIGN

There are many approaches being studied to create the contrast needed in the image plane of a telescope for exoplanet detection and characterization, most of which use either an internal coronagraph or an external occulter.¹ All approaches have the potential to yield similar exoplanet science (measured in number of planets discovered and characterized), yet each has different technical challenges. This TDEM focuses on an external occulter mission concept, a spacecraft containing a starshade with a shaped edge flown in formation with a telescope (see Figure 1), as a plausible mission architecture that could be flown in the next decade with limited technology development risk. The size, shape, and separation of the occulter are chosen so that it suppresses the light from the star by more than ten orders of magnitude over a particular wavelength band, while leaving the planet light unaffected. The *geometric inner working angle*, i.e., the closest angle at which a planet can be detected, is determined by the ratio of the occulter radius to its distance from the telescope. Most designs have the starshade tens of meters in diameter, and separated from the telescope by tens of thousands of kilometers, which gives the starshade an angular size less than 100 milliarcseconds.

Lyman Spitzer was the first to suggest using a smoothly apodized screen to block starlight (the apodization is critical as it limits light diffracting into the shadow area).² Recently, a number of approaches have been proposed for finding apodizations that produce sufficient starlight suppression.³⁻⁵ Unfortunately, it is virtually impossible to manufacture any smoothly apodized occulter with sufficient precision. We therefore approximate the apodized screen with a binary occulter, which allows either all or none of the light through at any point.^{4,6} The resulting shape has a series of petal-like structures along the edge, which vary in width with radius so that if a circle is drawn at a radius r , the fraction of the circle which is blocked by petals is $A(r)$, the desired apodization function. It can be shown that the resulting electric field is then the same as that of a smooth apodization, with a series of additional perturbation terms from the scattering due to the

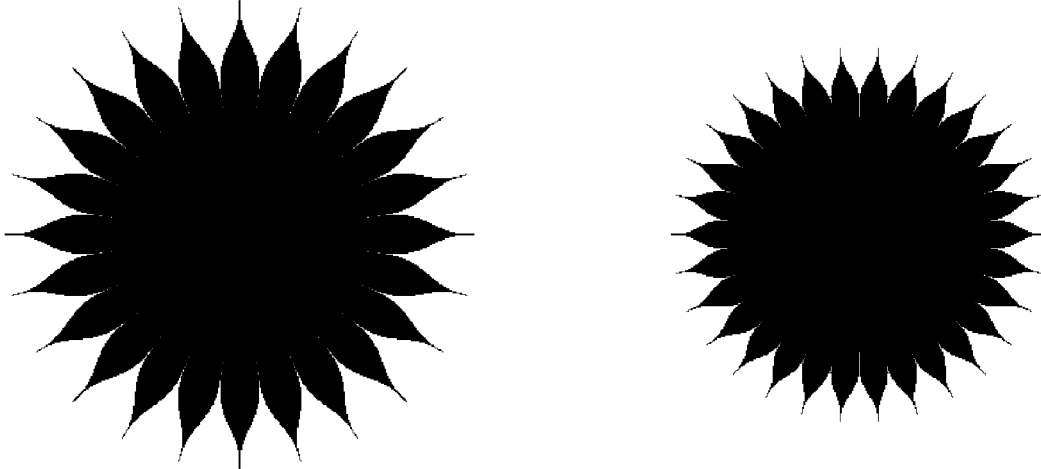


Figure 2. The *THEIA* occulter (left) and the DI22 starshade design (right).

petals.^{5,7} In our work, the occulter shape is determined using optimization methods.⁵ Recent variations of our optimization approach allow modifications to enhance manufacturability or otherwise simplify the design.⁸ We also reduce the size and distance of the occulter by leveraging the invariance of the Fresnel integral to the product of wavelength and distance to design the occulter to operate in two wavelength bands at two different distances.

We have studied the use of occulter for a variety of missions at different scales. For the 2009 Astrophysics Mission Concept Studies we developed the *THEIA* mission, or Telescope for Habitable Exoplanets and Interstellar/Intergalactic Astronomy, a flagship 4-meter on-axis optical/UV telescope with an external occulter for planet detection and characterization.⁹ The *THEIA* occulter is 40 m in diameter, with 20 petals, and is designed to work in two wavelength bands at different locations from the telescope: the 250-700 nm band at 55000 km, and the 700-1000 nm band at 35000 km. It has a geometric inner working angle of 75 mas at the furthest distance and 118 mas at the closest.

For this TDEM we chose to study an occulter designed for use with a 1.5 m telescope. The resulting starshade, which we refer to as DI22, is 32 m in diameter with 30 6 m petals and an inner working angle of 90 mas. Each petal has a width at the widest point of 2.34 m. It too operates over two bands, 250-550 nm at a distance of 36670 km and 500-1100 nm at a distance of 18335 km. It is shown in Figure 2 alongside the *THEIA* occulter.

3. REQUIREMENTS AND ERROR ANALYSIS

Designing the occulter through optimization is only the first step. Any realistic engineering design of the occulter can only meet the desired shape to within certain realizable tolerances. Additionally, the operation of the occulter through varying thermal environments and dynamic loading will inevitably cause variations in the shape. Shaklan et al.¹¹ describe in detail the modeling approach used to develop engineering requirements and determine the sensitivity of the design to errors in manufacture and variations in flight. An optical modeling tool has been developed, described there, that finds the image plane response of the telescope past an occulter with various errors. It is important to base all error budgeting on image plane simulations as different errors may diffract light to different locations in the image plane and thus have more or less impact on the ability to extract a close in planet.

Various types of perturbations have been analyzed, including petal size, bending, spatial frequency variations, positional variation, and tip errors. The various errors were accumulated into an error budget to allow requirements to be allocated to various sources. The final error budget was grouped into 8 categories:

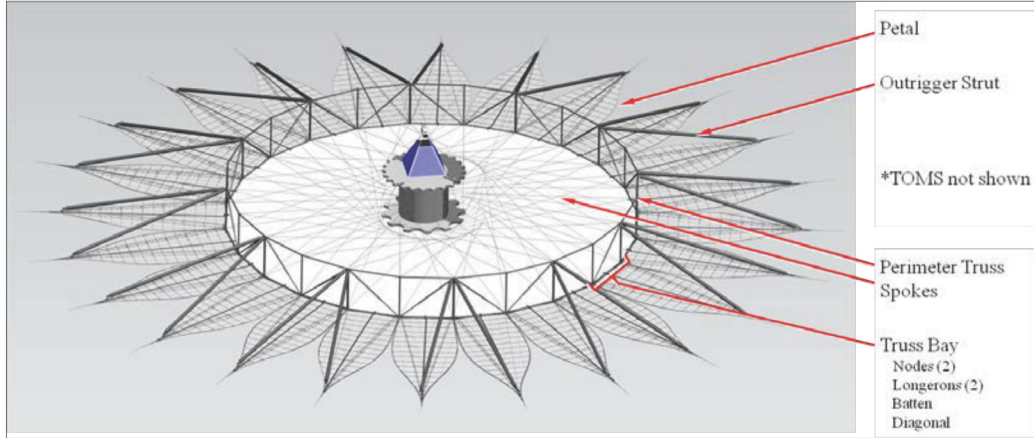


Figure 3. Diagram of deployed starshade including central hub, truss, and petals.

manufacture, deployed shape, deployed position, thermal, formation flying, dynamics, edge scatter, and reserve. As described earlier, edge shape error, the tall pole that we investigate in this TDEM, is allocated a contrast of 2×10^{-11} . The optical analysis shows that this is consistent with an rms error on the edges of approximately 28 microns. Indications from our current measurements is that the manufacturing process we are using is well within this capability. Another error of concern, edge scatter, has also been allocated a contribution of 2×10^{-11} , which is expected to be consistent with the edge having a 50 micron radius of curvature, pending detailed modeling and verification in the laboratory. The complete error budget can be found in Shaklan et al.¹¹

The current error budget and associated requirements assume a spinning occulter. By spinning the occulter, the contrast degradation due to edge errors is dominated by the mean shape of the edge rather than the rms variation, allowing almost a factor of 10 relaxation in the requirements. Spinning also averages thermal effects and minimizes dynamic errors.

4. STARSHADE MECHANICAL DESIGN

Our current mechanical design approach produces a starshade able to stow easily stacked on top of the telescope and thus fit in a common fairing. A schematic of the deployed design is shown in Figure 3. A deployable perimeter truss is used to form the inner disc and to provide a very stiff and stable interface for the petals. This design derives from the AstroMesh reflector antenna developed by Northrop Grumman Astro Aerospace (NGAS). The petals are arrayed around the circumference of the truss with only three kinematic (statically determinate) interface points: two at the base and one provided by a deployable outrigger strut. The petals employ a highly mass efficient lattice structure comprised of pultruded graphite fiber reinforced plastic (GFRP) rods that have finely tuned CTEs to limit thermal deformations. The lattice structure is configured and optimized to provide stiffness and stability as required to meet petal stability requirements. All deployments are passive using stowed strain energy for actuation, dampers for rate control and separately commanded release devices for sequencing.

When stowed, the starshade petals are wrapped around a fixed, lightweight central hub structure. The hub is sized to provide sufficient annular radius between its OD and the fairing ID to contain the stowed starshade truss and petals while maximizing hub diameter to reduce petal strain. For the 30m starshade design the hub can be about 3m in diameter. The petals wrap approximately 3/4 of the way around the hub circumferentially and overlap about 2/3 of the total stowed truss height vertically. The central hub provides space for the supporting spacecraft.

The perimeter truss is a very stiff, precise and stable deployed structure. The truss rim nodes are in turn the stiff interface points from which the petals are cantilevered, with additional support provided by



Figure 4. Deployment process of starshade.

a deployable outrigger strut for each petal. Each petal is precisely located in-plane to maintain the global figure profile by two latches, one at each corner of the petal root. The latches provide kinematic restraint of the petal in all degrees of freedom except rotation about the axis of the truss longeron adjacent to the root of the petal. This cantilever mode of motion is restrained by the deployable outrigger strut so the flat petal bodies remain aligned with the starshade plane. The result is that the petal/outrigger combination emulates a stiff tripod for structural efficiency. This is essential for achieving a low-mass structural system with high precision.

Figure 4 shows how the petals unfurl. Deployment during the first phase is entirely passive through the controlled release of stored strain energy. Unfurling is initiated by release of a belly-band restraint system around the circumference of the stowed starshade. Lanyards that play out from spools on passive rotary dampers and/or sequenced release devices such as pyros will meter the rate of unfurling. Once the petals are nearly straight, a pair of spring-loaded ribs pops open towards the sun-facing side of the petal to stiffen it and maintain flatness upon deployment. Deployment of the outrigger struts is concurrent with petal unfurling and is also achieved passively.

The final phase is deployment of the truss. Truss deployment is accomplished by reeling in a deployment cable on a motor-actuated spool. The cable runs around the circumference of the truss inside the telescoping diagonal members, which are extended when stowed. Spooling in the cable forces the diagonals to retract, which deploys the truss. Each bay of the truss is synchronized to its neighbor by synchronizer gear pairs that are attached to adjacent longerons at every other truss node. The petals simply follow the truss as it deploys to complete their 90° rotation into the plane of the starshade. When truss deployment is nearly complete all petal root latch pairs engage and latch to the truss nodes. The outrigger struts also latch in place, either passively or by commanding a single latch release device ganged to all outrigger latches via a cable. Truss deployment will be studied as part of the second follow-on TDEM.

The primary goal of this TDEM is the precision manufacturing and metrology of a single petal. Figure 5 details the petal structural design, as viewed from the telescope (anti-sun) side, with the Thermo-Optical Micrometeorite Shield (TOMS) blanket removed. The primary petal structure is a lattice of battens and longerons that intersect a longitudinal spine and a pair of structural edges on each side. These elements are optimized to place and precisely maintain the optical edge with the required profile tolerance regardless of thermal extremes or structural loads from the relatively thermally unstable TOMS. The lattice is highly mass efficient yet very stiff in-plane. Secondary petal structure includes a pair of deployable ribs in an A frame configuration that stiffen and maintain overall deployed petal flatness. The deployable ribs fold outward

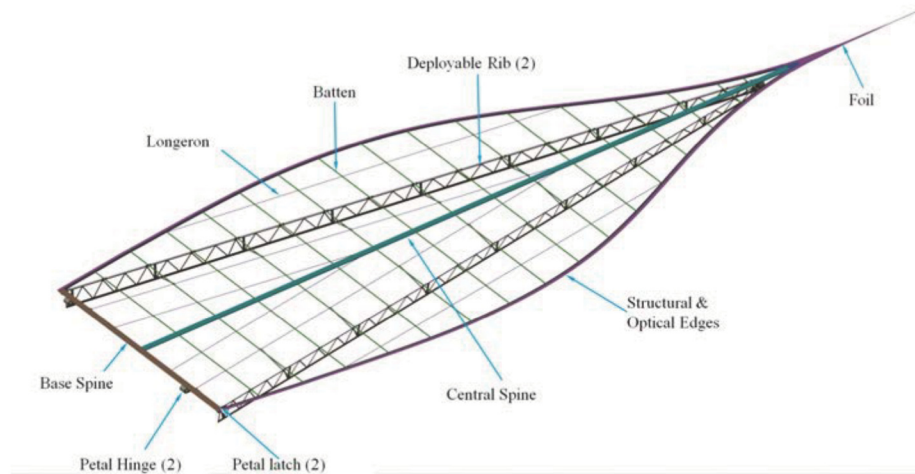


Figure 5. Schematic of petal mechanical design.

and flat against the petal when stowed then pop up into place when the petal is unfurling. The ribs are deployed by extension springs that are inside hollow soda-straw size GFRP struts that lock the ribs in place at a near-perpendicular angle to the petal when deployed. The ends of the deployable ribs coincide with truss-to-petal interface nodes on the base spine and with the outboard end of the outrigger at the apex of the “A” to complete the tripod-like geometry of the petal and outrigger support structure on the edge of the perimeter truss. The driver for sizing the ribs and battens is actually a 1-g petal gravity-sag displacement requirement of < 1.5 cm with the TOMS installed. This insures that a truss and petal alignment verification can be performed on the deployed starshade with high confidence prior to launch.

The battens define and maintain the precise petal edge-to-edge width. They are made from a pultruded GFRP base material that has a room-temperature axial CTE of better than $-0.2 \times 10^{-6}/^{\circ}\text{C}$. The battens are continuous across the width of the petal so that joints will not affect their axial stability. To maintain edge profile tolerances, the CTE of the batten base material is designed to nominally be zero using one or more of several proven strategies that will be selected during the planned development program. (The residual error in the CTE is incorporated into our thermal-mechanical modeling. At this early stage values are based on test data of standard commercial parts; eventually measured CTE values will be used which are expected to be much lower.)

Longerons provide the petal with in-plane shear stiffness for maintenance of the overall shape. They are made from the same pultruded GFRP as the battens, have a circular cross section and are also continuous along their length. The longest pair of longerons also act as hinge pins for the deployable ribs. The longitudinal and base spines provide additional stiffness and are constructed of a foam core sandwiched between thin graphite face sheets. The base spine closes out the petal root structure and carries the perimeter truss interfaces: two hinge points for the unfurling portion of deployment and two precise latches that position the deployed petal in-plane.

All petal structures are designed so that no component is subjected to more than 0.5% strain (5000 μstrain) when stowed around the 3m diameter hub; the critical shape-determining structures (such as the battens) are designed for $< 0.05\%$ strain. This design constraint insures that permanent plastic deformation or material creep that would degrade the deployed shape or figure of the starshade will not occur. This level of strain is only approached by the longitudinal spine in our current design, which has little or no role in the definition of the deployed petal edge profile. Its primary function is to accommodate launch restraints and deployment hardware and as a ground-handling interface. The battens are perpendicular to the direction of stowed petal strain and thus will not experience permanent set from material creep prior to launch.

Figure 6 shows an aluminum and composite engineering model petal before, during, and after deployment



Figure 6. Three images of an engineering model petal before, during, and after deployment from a test fixture. Standing left to right are Mark Thomson and Vinh Bach (left), Mark Thomson and Doug Lisman (center), Dan Barber, Mark Thomson, Rick Helms, Vinh Bach, Phil Walkemeyer, Doug Lisman, Otto Polanco (right).

from a test fixture that simulates the stowed package (all longerons and battens are made of composite carbon protruded rods, the spine facesheet is stainless steel and the pop-up ribs and edges are aluminum). This model was manufactured to verify the design approach and confirm the kinematic performance. It thus confirmed the design and will be used as a basis for manufacturing the flight-like composite petal. We also ensured that the residual strain levels are well within the design limits of composite materials. Through the deployment of the engineering model, appropriate analysis, and coupon testing we are confident that the petal made from flight-like composite materials will meet the deployment requirements. While deployment tests are nominally not part of this TDEM, our goal is to have the resources to perform a deployment test of the prototype petal and remeasure the edge shape.

We have performed preliminary thermal analyses of the mechanical design. Thermal deformations are potentially a significant source of petal shape error. The objective was to demonstrate that any shape variation due to thermal effects resulted in contrast that fell within the 2×10^{-11} allocation over a wide range of sun observing angles.

Solar incidence change is the primary source of uniform temperature deviations, which manifest as proportional width errors. Referencing the nominal shape to a temperature in the middle of the predicted range minimizes deformations. Petal shadowing is the primary source of non-uniform temperature deviations. At high solar incidence angles, petals can be fully shadowed and this manifests as a monotonic gradient. The inner disk has a warming influence on petals, but temperatures drop with increasing distance from the truss. Variable view factors, with some petal surfaces near normal to incident sunlight, or partially shadowed petals, are other sources of non-uniform temperature deviations, which manifest as semi-random deviations from the average batten temperature.

At high solar inclination angles the central hub casts hard shadows onto petals. Starting at lower solar inclinations, softer shadows are cast by the gossamer truss, open lattice pop-up ribs and pyramid shaped solar array. The diagram in Figure 7 shows the geometry for shadows cast by the central hub. The petal directly opposite the sun direction starts to be shadowed by the central hub at around 70° solar incidence and is fully shadowed by about 80° solar incidence. For a spinning occulter operating at large solar incidence angles, all petals will periodically pass through the shadow cast by the central hub. This calls for a transient thermal analysis.

The table in Figure 7 summarizes the results of our steady state and transient analyses. It shows robust margins relative to allocations. The reference design is fully compliant with thermal deformation requirements. It is also important to note that we have incorporated significant margin into the analyses by using a higher CTE than we believe can be achieved, by incorporating a larger solar inclination angle range than required, and by assuming a higher temperature deviation than we expect from our selected blanket emissivity. This indicates substantial robustness in the design and shows that no new technology development is needed to meet thermal stability requirements. Requirements are satisfied with the baseline design using commercially available materials. A lower CTE is desirable and readily achievable with proven technology.

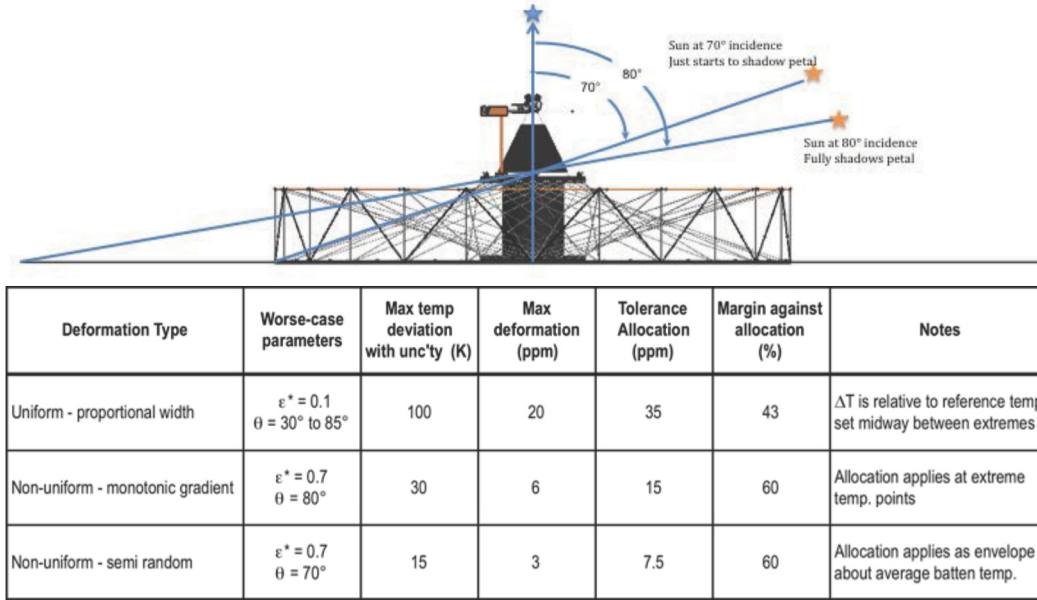


Figure 7. Geometry for steady-state and transient thermal analysis including shadowing (top) and expected deformations due to thermal variations (bottom).

5. METROLOGY

Metrology is performed at several stages in the petal build process. The coordinate measuring machines (CMMs) used are limited to what is either currently available at JPL or is available at local vendors. We note that producing a large number of flight petals will require a customized tool at the production site. The measurements are supported by a large number of targets, called buttons, that are installed on the petal structure and the optical edge segments.

The first metrology step is to measure button positions on the assembled structural petal using a spherical ball probe; this step has been completed. This step was performed at Allied Mechanical using a large gantry style CMM. Three sets of measurements demonstrate a positional variance of less than 5 microns.

The second metrology step is to measure both the button positions and the edge profile of the optical edge segments; this step is currently in progress. This step is being performed at Hexagon Metrology using a smaller gantry style CMM with both a spherical ball probe (for button cones) and an optical sensor (for edge profile at high frequency). The optical and mechanical sensors are accurately coaligned on a measurement target so that minimal offset is expected between the optical and mechanical measurements.

Metrology data from steps one and two are analyzed to determine the optimal position of each optical edge segment, which minimizes the residual mean petal width error. The optimal position is specified in terms of buttons installed on the two ends and middle of each petal, relative to buttons installed on the adjoining structure. The Faro CMM tool (shown in Figure 8) is used to measure these button positions. The position is adjusted using micrometer stages in close proximity to the three edge segment buttons. After achieving the desired position, the edge segments are clamped in place, using custom designed pneumatic clamps that apply minimal side load, and then bonded in place. The third metrology step is measuring the petal width, using the Faro CMM tool, after edge installation is complete.

The fourth metrology step is to independently verify the final petal shape. This step is performed at Allied Mechanical using the same CMM as in the first step. The buttons are remeasured with a spherical ball probe and the optical edge position is measured with a cylindrical probe. Three sets of data will be collected to establish repeatability. At that point, all of the data necessary to address the milestone are available.



Figure 8. The calibrated metrology ball (top left), Faro arm for calibration (top right with with Stefan Martin and Vinh Bach), and Faro arm in use during assembly (bottom with Vinh Bach).

6. MANUFACTURING PROGRESS

Figure 9 shows a flowchart of our TDEM manufacturing and metrology plan. The production strategy for establishing the figure profile is to first fabricate the deployable petal structure rapidly and for the lowest possible cost without utilizing high-precision tooling or metrology. This is not only to support current TDEM goals but also to minimize the cost of the ultimate flight article. The optical edges are added later so the deployable petal structure need not be fabricated to a high degree of precision; it must simply be made of stable materials. The petal structure is assembled to a modest degree of accuracy, about 250 micron, as readily achievable with tools on-hand, including use of the FARO arm.

To date we have completed procurement and layup of the composite material, manufacture of the structural parts, assembly of the mechanical structure, and metrology on the mechanical edge. Figure 10 shows three images of the assembly process. Figure 11 shows the final assembled mechanical structure before shipment to Allied Mechanical Corp. for shape measurement. Edge measurements had a repeatable accuracy of better than 5 microns.

The 25mm wide and 0.4mm thick graphite composite optical edges have been manufactured separately from the petal in the longest lengths practical for maintaining the required figure profile; between 0.8m and 1.3m long. The segments will be aligned using micrometer stages and then secured with precision clamps for a room temperature cure bonding process. The petal tip is bolted into a transition plate that connects the central spine and edges together. (Note that the petal tip is not being manufactured or attached to the needed precision for this TDEM.)

Figure 12 shows a half-size edge test piece. Based on the success of this test piece, the final edge segments entered manufacture. They have just completed machining and are currently being measured. Installation to the petal is expected to begin soon. The original plan was for the optical edges to also contain the small

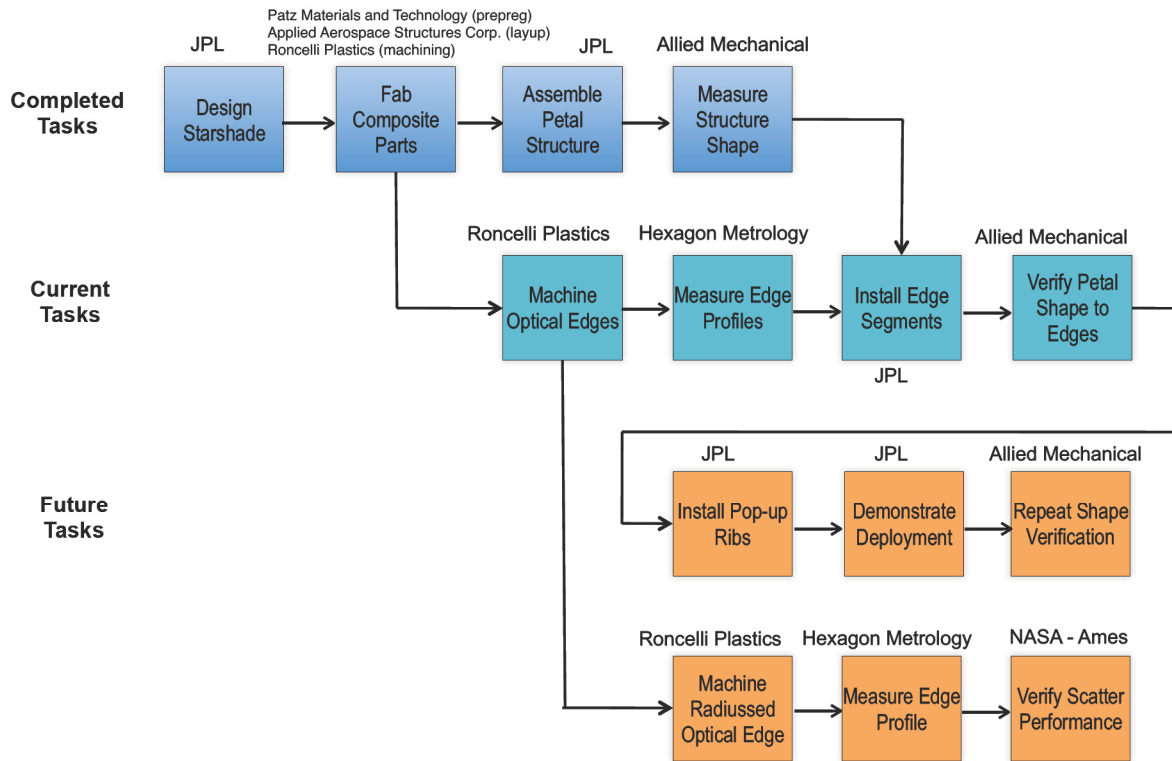


Figure 9. A Workflow chart of the TDEM activities highlighted work completed to date, current activities and planned future tasks.

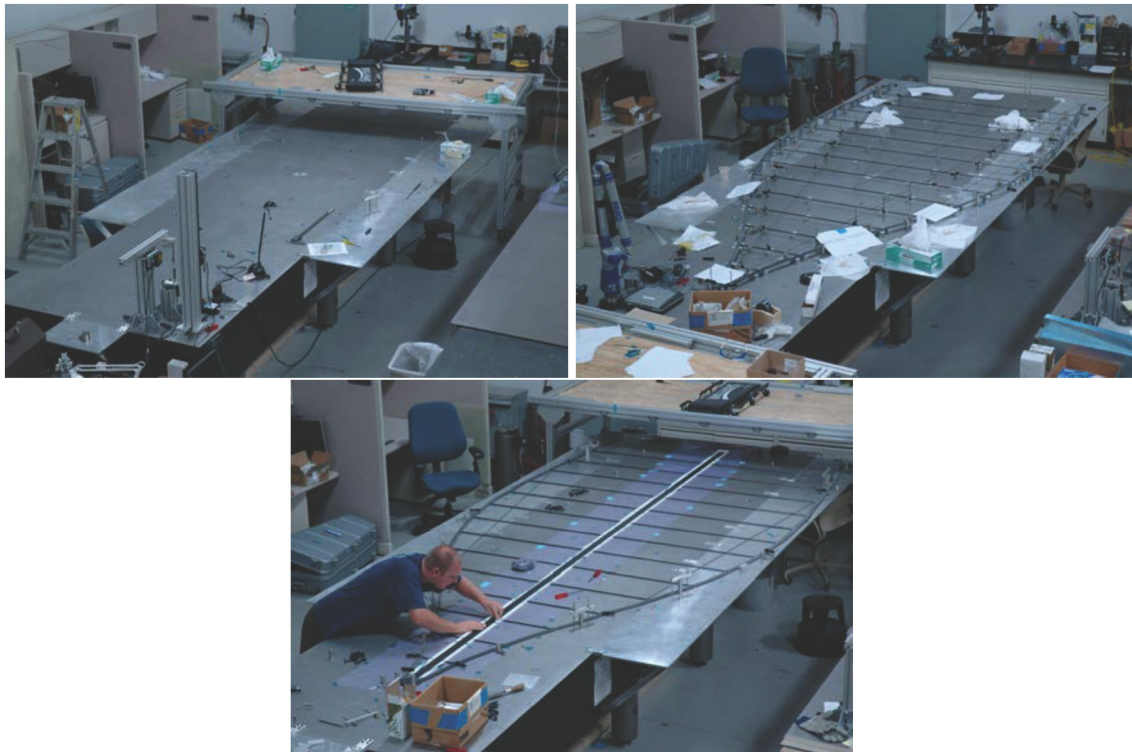


Figure 10. Three images of the assembly process of the petal mechanical structure (shown in bottom is Eric Oakes).



Figure 11. Final assembly of the petal mechanical structure without optical edge.

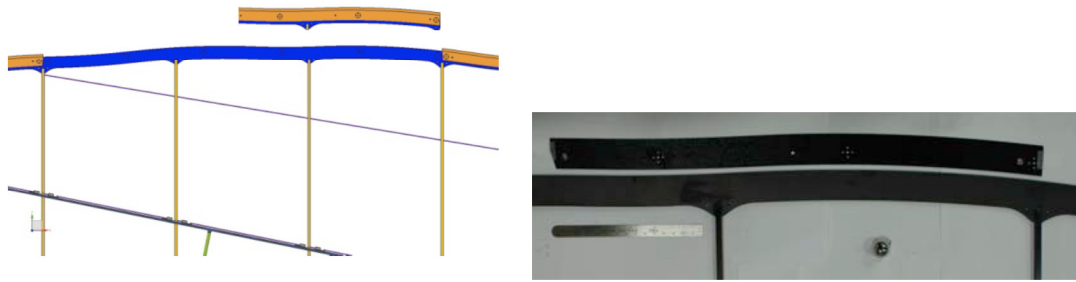


Figure 12. Diagram of edge segment location (left) and test sample of optical edge along assembled mechanical structure (right).

radius of curvature necessary to prevent solar glint. This proved to be a difficult manufacturing challenge and we decided to instead make flat optical edges for this first TDEM petal. This both separates the two development paths and simplifies the metrology. A contact measurement system, such as the CMMs we plan for the petal width measurements, would be extremely difficult to use on the sharp edges and very sensitive to alignment and placing. We are in parallel exploring various sharp edge production techniques and plan to produce various test samples to be used in optical scatter tests at the NASA Ames Research Center. We also note that in future development phases or final flight article production we expect that a custom laser metrology system with optical edge sensing would be used for aligning the optical edge segments on the petal structure. The metrology system would be integrally mounted on a large graphite composite bench that is in a tightly controlled environment. This eliminates the problems of contact with the sharp edge.

7. FINAL REMARKS

We are on schedule to complete the objectives of our first phase TDEM program before the end of the year. In fact, we expect to exceed our requirement and meet our goal of 2×10^{-10} contrast due to static manufacturing error. We also hope and expect to beat our schedule and have the time and resources to perform a deployment test of the composite petal with a post-test measurement. We have also developed a flight level error budget and performed initial thermal analysis to shows that the design meets requirements. Within the cost and schedule constraints of the TDEM program we have demonstrated that we can design, build, and measure flight like petals to levels consistent with detecting Earth-like planets, retiring all of the manufacturing risk.

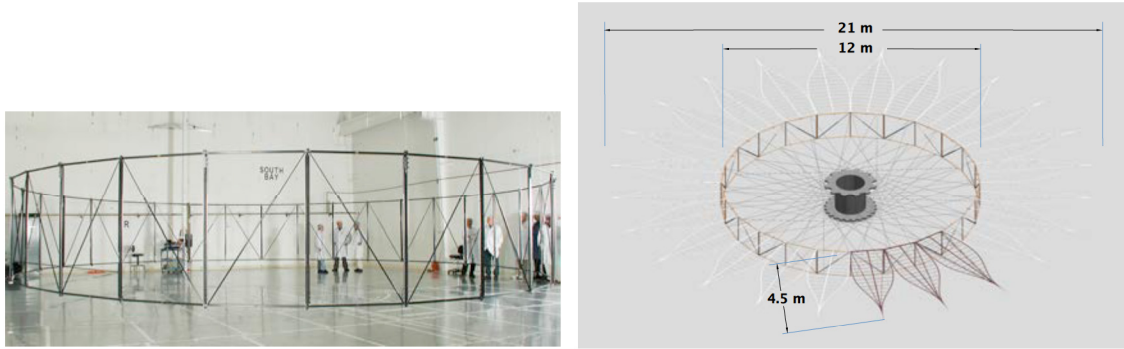


Figure 13. Existing deployable truss (left) and diagram of proposed three petal deployment (right).

We were also recently notified of our selection for the second TDEM phase. In that we plan to verify starshade deployment functionality and interfaces by demonstrating repeated deployment of a 3 petal and truss subscale prototype consistent with a total instrument contrast of 10^{-10} (< 0.5 mm). Figure 13 shows an existing deployable truss at Northrop-Grumman’s Astro division that will be modified for the TDEM. Also shown is a diagram of the three engineering model petals in the deployment position on the truss. We plan to use photogrammetry to measure the deployment accuracy on repeated stow and deploy cycles.

Acknowledgements

This work was partially performed under a grant from the National Aeronautics and Space Administration (NASA), grant number NNX10AF83G. This work was partially carried out at the Jet Propulsion Laboratory, California Institute of Technology, under contract to NASA. The work of Macintosh and Rudd was performed under the auspices of the U.S. Department of Energy by Lawrence Livermore National Laboratory under Contract DE-AC52-07NA27344.

REFERENCES

1. S. V. W. Beckwith, “Detecting life-bearing extrasolar planets with space telescopes,” *The Astrophysical Journal* **684**(2), pp. 1404–1415, 2008.
2. L. Spitzer, “The beginnings and future of space astronomy,” *American Scientist* **50**, pp. 473–484, 1962.
3. C. Copi and G. Starkman, “The big occulting steerable satellite [BOSS],” *Astrophysical Journal* **532**, pp. 581–592, 2000.
4. W. Cash, “Detection of earth-like planets around nearby stars using a petal-shaped occulter,” *Nature* **442**, pp. 51–53, 2006.
5. R. Vanderbei, E. Cady, and N. Kasdin, “Optimal occulter design for finding extrasolar planets,” *Astrophysical Journal* **665**, pp. 794–798, 2007.
6. W. L. Simmons, “A pinspeck camera for exo-planet spectroscopy.” Princeton University Master’s Thesis, 2005.
7. R. Vanderbei, D. Spergel, and N. Kasdin, “Circularly symmetric apodization via star-shaped masks,” *Astrophysical Journal* **599**, pp. 686–694, 2003.
8. E. Cady, S. Shaklan, N. Kasdin, and D. Spergel, “A method for modifying occulter shapes,” *Techniques and Instrumentation for Detection of Exoplanets IV* **7440**, SPIE, 2009.
9. N. J. Kasdin, P. Atcheson, M. Beasley, R. Belikov, M. Blouke, E. Cady, D. Calzetti, C. Copi, S. Desch, P. Dumont, D. Ebbets, R. Egerman, A. Fullerton, J. Gallagher, J. Green, O. Guyon, S. Heap, R. Jansen, E. Jenkins, J. Kasting, R. Keski-Kuha, M. Kuchner, R. Lee, D. J. Lindler, R. Linfield, D. Lisman, R. Lyon, J. MacKenty, S. Malhotra, M. McCaughrean, G. Mathews, M. Mountain, S. Nikzad, B. O’Connell, W. Oegerle, S. Oey, D. Padgett, B. A. Parvin, X. Prochaska, J. Rhoads, A. Roberge, B. Saif, D. Savransky, P. Scowen, S. Seager, B. Seery, K. Sembach, S. Shaklan, M. Shull,

- O. Siegmund, N. Smith, R. Soummer, D. Spergel, P. Stahl, G. Starkman, D. K. Stern, D. Tenerelli, W. A. Traub, J. Trauger, J. Tumlinson, E. Turner, B. Vanderbei, R. Windhorst, B. Woodgate, and B. Woodruff, "THEIA: Telescope for habitable exoplanets and interstellar/intergalactic astronomy." http://www.astro.princeton.edu/dns/Theia/nas.theia_v14.pdf.
10. D. Savransky, N. Kasdin, and D. Spergel, "Results from the automated design reference mission constructor for exoplanet imagers," *Techniques and Instrumentation for Detection of Exoplanets IV* **7440**, SPIE, 2009.
 11. S. B. Shaklan, L. F. Marchen, D. Lisman, E. J. Cady, S. R. Martin, N. J. Kasdin, and P. J. Dumont, "A starshade petal error budget for exo-earth detection and characterization," in *Proceedings of the SPIE Conference on Optics and Photonics*, 8151(38), 2011.